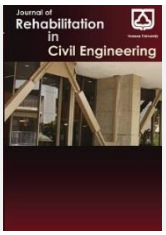

Journal of Rehabilitation in Civil Engineering

Journal homepage: https://civiljournal.semnan.ac.ir/

Evaluation of Steel Frame Equipped with the Replaceable Shear Link Made of Shape Memory Alloy under the Impact Load

Reza Kamgar [1,*]; Seyed Ali Mahmoudy [2]; Roham Zakavi [3]

1. Associate Professor, Civil Engineering Department, Faculty of Engineering, Shahrekord University, Shahrekord, Iran
2. M.Sc Graduated, Department of Civil Engineering, University of Isfahan, Isfahan, Iran
3. M.Sc Graduated, Department of Civil Engineering, Shahid Bahonar University of Kerman, Kerman, Iran
* Corresponding author: *kamgar@sku.ac.ir*

ARTICLE INFO

Article history:
Received: 05 February 2023
Revised: 29 September 2023
Accepted: 31 December 2023

Keywords:
Impact load;
Shear link;
Framed tube;
Shape memory alloy;
Nonlinear dynamic analysis.

ABSTRACT

Despite their low stiffness, moment frames (MFs) are considered conventional lateral strength systems for low- and moderate-rise structures due to their ability to absorb energy and provide suitable ductility, along with architectural considerations. In return, a framed tube system with deep beams and short spans suits the high-rise structures. Due to the differences between the span length-to-depth ratios of the beams in this structural system, the regulations for MFs cannot apply to them. Moreover, a low value for the length-to-height ratio of the beams prevents the proper formation of flexural plastic joints proposed by the regulations. Therefore, a frame with a single story and span has been proposed here consisting of a replaceable shear link made of shape memory alloy (SMA) to study the responses of the structure under the explosive loads (i.e., lateral loading) that can occur due to terrorist attacks, industrialization, or mining actions. Therefore, this study investigates the behavior of different systems under the three types of impact loads, including SMA or steel shear links. The results show that in the frame equipped with a shear link made of an SMA, the base shear is less than that of ordinary steel (the maximum base shear reduction is about 27% for type 2 blast load). This leads to a reduction in the cost of foundation construction. Also, the maximum displacement in the frame equipped with the shear link made of ordinary steel is less than the corresponding value in the frame equipped with a shear link made of an SMA (the maximum displacement reduction is about 43% for type 1 blast load), while the residual displacement of both frames is the same and equal to zero. It was concluded that the free vibration does not significantly affect the maximum responses of the mentioned structures under the impact load.

E-ISSN: 2345-4423

How to cite this article:
Kamgar, R., Mahmoudy, S. A., & Zakavi, R. (2024). Evaluation of Steel Frame Equipped with the Replaceable Shear Link Made of Shape Memory Alloy under the Impact Load. Journal of Rehabilitation in Civil Engineering, 12(4), 66-85. https://doi.org/10.22075/jrce.2023.29623.1806

1. Introduction

Due to the increase in terrorist attacks, several studies have been conducted on the load of explosions and how to reduce the effects of explosive loads on structures [1–3]. Structures movements due to explosion and impact include short-duration and high-frequency movements. According to such unique features, the response of the building to such loads is very different from the response to an earthquake load [4]. Also, the research on the qualitative effect of high-frequency excitations with short duration and large magnitude on the structure's response still needs to be completed. The experimental studies on the reinforced concrete beams subjected to the blast load have been performed by Magnesa. In Magnasa's research, dynamic analysis was performed using the single-degree-of-freedom system and damage curves. He compared the results obtained from the dynamic response of the supports with the experimental ones. He indicated that shear failure occurs for a reinforced beam with a high percentage of tensile rebar, while the failure mode has changed for a beam with a lower percentage of rebar [5]. After that, Baker *et al.* examined several models for calculating overpressure and impact caused by industrial explosions and introduced the equivalent TNT model. Finally, they introduced curves by which the equivalent TNT value, the relationship between overpressure, distance, and impact, can be estimated [6]. Ngo *et al.* analyzed the behavior of high-strength (HSC) columns under the blast load. They showed that the shear failure mode governing the fracture mode for explosion occurs near the column. They concluded that the HSC columns performed better than conventional columns when exposed to heavy blast loads. Furthermore, they show better energy absorption, as seen in the HSC columns [4]. Luccioni and Luege examined a sample of common concrete bridges with two spans and lines with AASHTO type III beams. This study analyzed beams and columns under the explosion load. The results indicated that girders, designed according to AASHTO, did not have the necessary ability to resist the explosion load [7]. Shi *et al.* showed that using the AUTODYN software to accurately model the blast wave in interaction with reinforced concrete columns, the dimensions and geometric shape of the columns significantly affect how the blast wave and load propagate on the columns [8]. LS-DYNA is another common software for blast modeling investigated by Hao *et al.* This software numerically simulates the gradual collapse of a reinforced concrete structure under blast load [9]. Recently, Kamgar and Shams investigated the nonlinear response of buckling-restrained braced frames under explosion load [10]. Also, the optimum location of a passive control system (i.e., outrigger belt truss system) has been found by Tavakoli *et al.* for a tall structure under the blast load [11]. In investigating the effect of explosion load on structural components, Bahirati *et al.* utilized ANSYS software to assess the effect of explosion load on the response of concrete slabs [12]. Amini *et al.* [13] employed the quartic B-spline time integration method to solve the nonlinear dynamic analysis of a single-degree-of-freedom system under exploding loads. Recently, some researchers have studied the weight optimization and relative lateral displacement of structures under the blast load [14,15]. Heidari-Mal Amiri and Tavakoli [16] analyzed the behavior of rectangular columns made of different FRP and steel rebars under impact loading. Kamgar *et al.* [17] evaluated the response of an elastic-plastic single-degree-of-freedom system under different explosion loads with different positive phase durations. Their results demonstrated that the maximum displacement and ductility of the system would increase by increasing the positive phase duration. The behavior of CFDST columns under different blast loading conditions was examined using numerical and experimental studies by Li *et al*

[18]. In 1969, Fazlur Khan first classified the existing tall buildings based on their height and structural performance. Therefore, the first step in creating a versatile structural system for tall buildings occurred. The framed tube system is the first type of tubular structural system that Fazlur Khan used to build tall buildings. In this system, the external walls consist of beams and columns close to each other, connected with rigid connections and deep perimeter beams. Therefore, it can resist lateral loads without using bracing. This system is quite effective, and its economy depends on factors such as columns' spacing and size, perimeter beams' depth, and the building plan's dimensional ratio [19,20]. In other words, a framed tube is a resistant lateral system that employs the entire perimeter of the building. In practice, in the framed tube, the columns are connected at a distance of 4 to 6.1 meters using perimeter beams with a depth of 0.9 to 1.52 meters. This system is economical for steel buildings up to 80 meters and concrete buildings up to 60 meters. So far, different studies have been performed on the seismic performance evaluation of this structural system under static load [21,22], wind load [23], and earthquake load [24].

Today, much civil engineering research focuses on reinforcing structures against lateral loads. The main two factors in forming new methods and materials are increasing the mechanical properties (e.g., bearing capacity, ductility, and energy absorption of the structure) and improving the structure's performance by reducing the damage value. Steel shear walls are suitable structural systems with high stiffness, strength, and energy absorption but low resistance to fire [25]. After using new materials such as FRPs and steels with low yield points in the main structural members [26–30], shape memory alloys with high ability in ductility have recently been utilized [31,32]. SMA is a steel alloy that can return to its original state after major deformation. In fact, reversibility can occur by applying heat or removing stress, representing the shape-memory and ultra-flexibility features, respectively. Based on these suitable properties of SMA, it is used in different parts of structures (e.g., SMA braces in modular steel frames [33], SMA bolts, or SMA angle in collector beam to link beam connection for eccentrically braced frames [34,35], and SMA bolts in steel coupling beams [36]) to meet the seismic resilient concept and decrease the residual deformations of the system. Moreover, SMA rods were recently utilized in link beams such as eccentrically braced frames and coupled core wall systems [37]. In another study, NiTi shape memory alloy panels were tested under cyclic shear loading [38]. Also, the researcher has studied NI-Ti shape memory alloy on the responses of steel plate shear walls [39].

Some studies focus on evaluating the performance of SMA materials under the blast load. Wei and Vigh [40–43] investigated the behavior of smart connections consisting of Nickle Titanium Shape Memory Alloy bolts under blast loading. Their results with this type of connection showed a reduced inter-story residual drift ratio compared with the steel-bolted connection. Based on previous literature, there is no research to investigate the explosion's impact on the behavior of SMA replaceable shear links.

This paper investigates the behavior of the framed tube equipped with the replaceable shear link. Figure 1 shows the main steps of the paper. For this purpose, the modeling validation and numerical behavior of the steel frame with the shear link are first studied using ABAQUS finite element software [44]. Therefore, Cheng’s model [45] is considered here and verified. Then, shaped memory alloy materials were used to evaluate the performance of this type of structural system under three explosion loads. In other words, the structure's response with SMA shear and steel shear links, including base shear, displacement versus time, and the Von-Mises stresses created in the structure, were obtained and discussed. Generally, the stresses and base shear of a structure equipped with SMA are lower than those values in a structure made of

steel. On the other hand, the structure's displacement with SMA is higher than that value in the structure with steel, while both considered systems have the same residual displacement values.

In conclusion, for the SMA structure compared to the steel structure, lower base shear and stresses make the structure and foundation light, while the deformation of the structure is increased, and the cost of the SMA itself is relatively high. Therefore, using SMA in some parts of the structure that absorb more energy is better and more economical. Accordingly, engineers should use this type of structure according to their needs, goals, and project conditions.

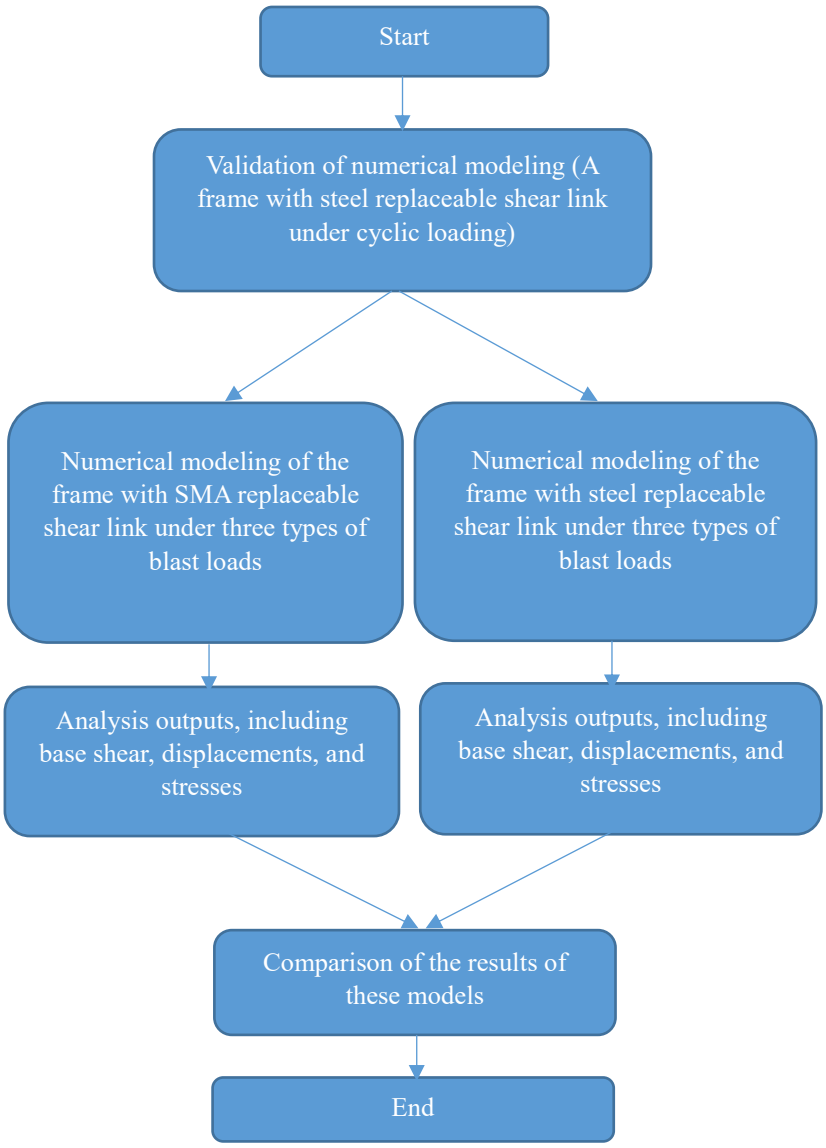

Fig. 1. The main steps of the paper.

2. Model introduction

An experimental sample is selected here to model in the ABAQUS software [44]. Figure 2 depicts the details and geometric characteristics of the experimental sample. In this model, the H360×226×12×16, H400×148×10×12, and H220×130×8×10 steel sections are used for columns, deep beams, and shear links, respectively. The total frame height from the support to the load location, the center to the center of the columns, and the length of the shear link beam are 2200 *mm*, 2000 *mm*, and 400 *mm,* respectively. This paper utilizes the bottom and top plates to connect the deep beams to the

column. The end plates connect the shear link to the deep beams with a screw connection.

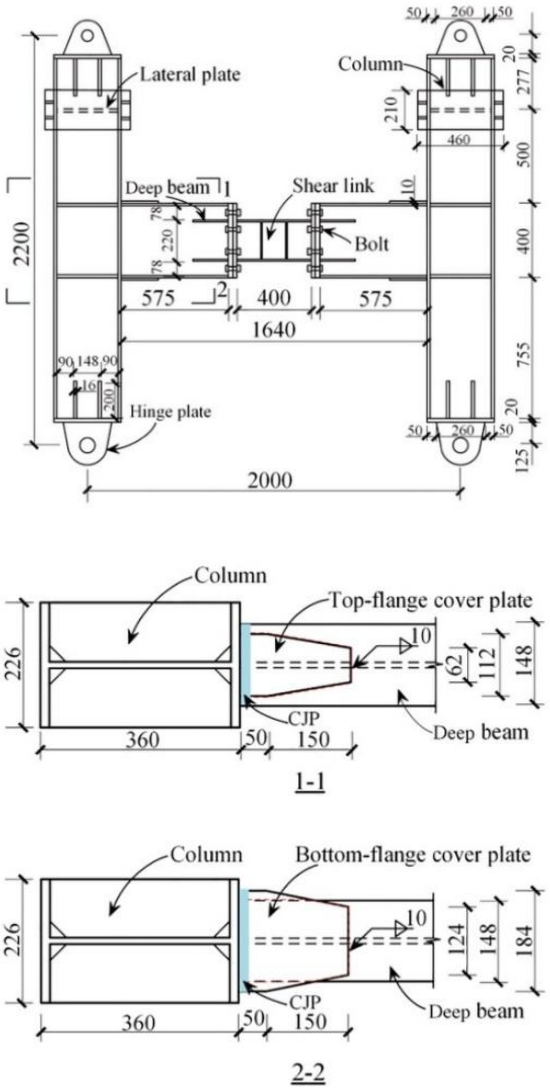

Fig. 2. Geometric characteristics of the studied experimental sample [45].

Finally, deep beam and column elements have the "Q460 steel material" with a nominal yield stress of 460 MPa. This material is chosen here to have a similar mechanical property to ST37. Also, SMA materials have similar properties to selected steel, so the comparison is possible. Also, Q235 steel material with a nominal yield stress of 235 MPa is utilized for shear links. Table 1 shows the tensile test results for steel with different thicknesses.

where t represents the thickness, E shows the modulus of elasticity, σ_y depicts the yield stress, σ_u is the final stress, and ε_y displays the yield stress.

3. Numerical modeling

This study uses the ABAQUS finite element software to investigate the performance and nonlinear behavior of replaceable shear links subjected to the lateral load. Figure 3 illustrates the finite element model of the considered structure.

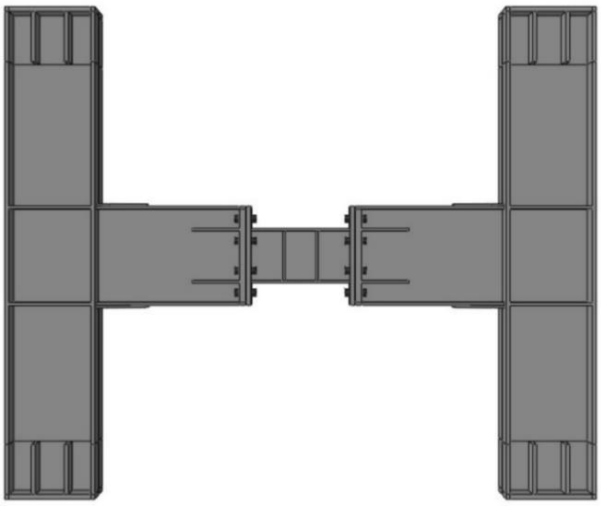

Fig. 3. Finite element model of steel frame with interchangeable shear link.

Table 1. Tensile test results for steels of different thicknesses

Steel Type	t (mm)	E (GPa)	σ_y (MPa)	σ_u (MPa)	σ_y/σ_u	ε_y $(\times 10^{-6})$
Q235B-8	*7.89*	*200*	*287*	*430*	*0.67*	*1435*
Q235B-10	*9.9*	*201*	*290*	*428*	*0.68*	*1443*
Q460C-10	*10.23*	*195*	*547*	*611*	*0.90*	*2805*
Q460C-12	*12.09*	*195*	*616*	*695*	*0.89*	*3159*
Q460C-16	*16.08*	*203*	*621*	*670*	*0.93*	*3059*

4. Material specifications

Figure 4 illustrates the materials utilized for the column and deep beam in the ABAQUS software [44]. Also, according to the experimental results [45] and the distribution of plastic stresses in the shear link, the Chaboche model is utilized to introduce the strain stiffness of the material. Table 2 shows the parameters of the considered model. The Chaboche model can consider plastic joints.

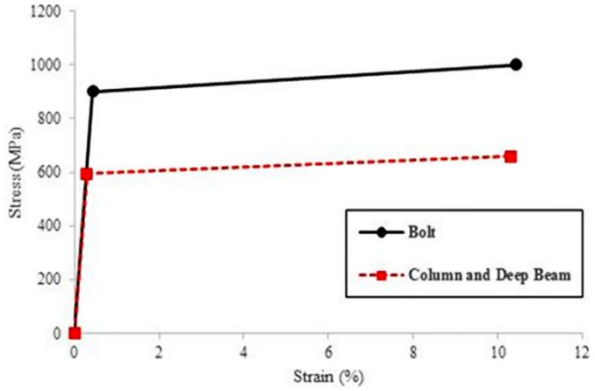

Fig. 4. Bi-linear strain stress curve of steel used for bolts, beam, and column elements.

Table 2. Calibrated parameters of the Chaboche model [29,46,47].

Steel Type	σ|0 (MPa)	Q∞ (MPa)	biso	Ckin,1 (MPa)	γ1
Q235B-8	270	20	1.2	6000	200
Ckin,2 (MPa)	γ2	Ckin,3 (MPa)	γ3	Ckin,4 (MPa)	γ4
5000	200	3000	70	990	40

5. Solver selection and meshing

All loads have been defined here in three steps. The first step applies the prestressing force to the bolts using the "BOLT LOAD" function in the ABAQUS software. In the second step, a gravitational load is applied to the structure. Finally, the explosion load is defined and applied in the third step. Since the present study includes the dynamic load due to the explosion load, an implicit solver is utilized in the finite element model, and the dynamic analysis type is implicit. Also, a standard solver is used to apply the prestressing load in the first step, and the General static load is used to solve it. It should be noted that the geometry's nonlinear effects are also considered.

For meshing purposes, the eight-node brick element with reduced integration ("C3D8R" solid elements) that can control the hourglass phenomenon is used here to model the components of the desired bending frame, including beams, columns, connecting plates, bolts, and nuts. The structured mesh technique was used to mesh the column, deep beam, and end plate. Also, the sweep mesh technique was used to mesh cover plates and shear links. Both mentioned techniques were employed for the modeling of bolts. The column, deep beam, bolt, and shear link element mesh sizes are 40, 25, 5, and 20 *mm*, respectively. These dimensions have been considered based on the try-and-error method. In fact, the mesh dimensions are decreased from large to small to find the optimum mesh with high accuracy and minimum computational cost. Figure 5 shows the meshed model of the studied structure.

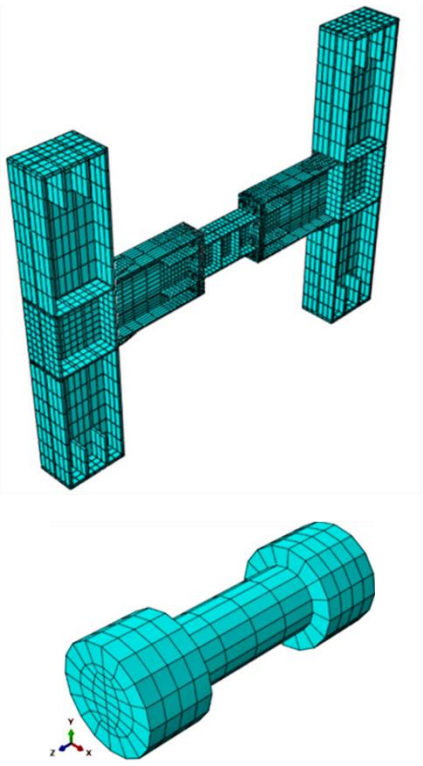

Fig. 5. The meshed model of the studied structure and bolt.

6. Interactions and boundary conditions

The finite element model uses the "Tie" constraint to connect the elements and simulate welding. Contact interaction is also used to connect the bolts with the end plate holes and the contact surface between the two end plates. In this research, the contact interaction in the perpendicular direction is considered hard contact. Also, the columb friction, with a coefficient of friction of 0.35, is used for the tangential direction [45,48]. According to Figure 2, the coupling constraint is utilized to simulate the connection of the columns to the supports and the upper rigid beam. Since the pin connection was used to connect the columns to the base in the experimental test, in the finite element model, only the transitional degrees of freedom are constrained (U1=U2=U3=0). Also, to simulate the two-dimensional behavior of the structure, in the finite element model, the degrees of freedom perpendicular to the web of the beams are constrained (i.e., U1=UR2 =UR3= 0).

7. Loading condition

In this paper, the surface blast load is applied to the structure. Based on Kamgar *et al.* [17]and Amini *et al.* [13] three blast loads with different positive phase durations (i.e., 0.5, 1.5, and 5 μsec) are considered here to investigate the effects of changing the positive phase duration on the responses of the studied structure. In fact, the equation utilized to compute the blast load has been considered based on Refs [13,17]. It should be noted that all considered blast loads have the same maximum intensity (i.e., 294300 *N*) and total time (i.e., 8 μsec). Also, all considered loads are located at different distances from the structure; therefore, the amount of positive impact will be different by assuming different positive phase durations. In the first case, the explosion load on the structure is calculated from equation $P(t)_1 = 294300 \times (1-2t) \times e^{-(\frac{5t}{6})}$ *N*. The positive phase duration and the positive impact are equal to $t_d = 0.5\ \mu$sec and $6.4338 \times 10^4\ (N.\mu \text{sec})$, respectively. In the second case, the blast load imposed on the structure is calculated from the equation $P(t)_2 = 294300 \times (1-\frac{2t}{3}) \times e^{-(\frac{5t}{6})}$ *N*, and the positive duration phase is $t_d = 1.5\ \mu$sec. In this case, the blast load's positive impact is equal to $1.5158 \times 10^5\ (N.\mu \text{sec})$. In the third state, the blast load is calculated from the equation $P(t)_3 = 294300 \times (1-\frac{t}{5}) \times e^{-(\frac{5t}{6})}$ *N*. In this state, the positive phase duration and the amount of positive impact are $t_d = 5\ \mu$sec and $2.6972 \times 10^5\ (N.\mu \text{sec})$, respectively. Figure 6 illustrates the time history of the explosion load.

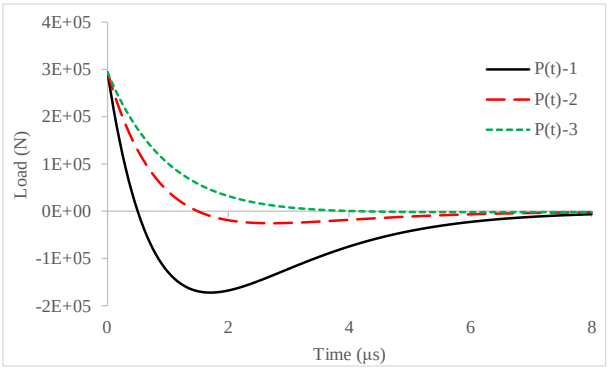

Fig. 6. Time history of different explosion loads (i.e., 1, 2, and 3).

8. Results and discussion

Figure 7 compares the experimental hysteresis diagram of the frame under cyclic loading [45] with the results of numerical modeling performed in the ABAQUS software [44]. As shown in Figure 7, the results of the numerical study have an excellent convergence with the experimental ones, and the maximum error value is 10%. In other words, the biggest difference between the diagrams is at the end of the curves, where the end of the numerical curve in the positive phase is almost

associated with 360 *tons* and 3.3% drift. In contrast, the experimental curve is almost associated with 400 *tons* and 3.3% drift. Also, in Figure 8, a comparison between the experimental and the numerical samples shows a good agreement.

It should be mentioned that the verification based on the cyclic load, considering both tensile and compressive loads, can show the basis of the model's accuracy. After that, the behavior of the structure under the blast load with a push in a fraction of a second can be checked. In addition, the strain rate created in SMA and steel due to blast load can be correctly simulated with ABAQUS software, according to Refs [49–52]. In fact, this paper initially investigated the model's accuracy in tension and compression zones under a cyclic load. After verification (see Figure 7), the blast load is applied to the model. It should be noted that blast loads have two parts (i.e., positive and negative phase durations). Therefore, it needs to check all tension and compression zones. The difference is for the duration of the compressive load, with a time scale of microseconds. It takes smaller time steps to perform a nonlinear analysis for the structure subjected to the blast load than the cyclic load, which is time-consuming.

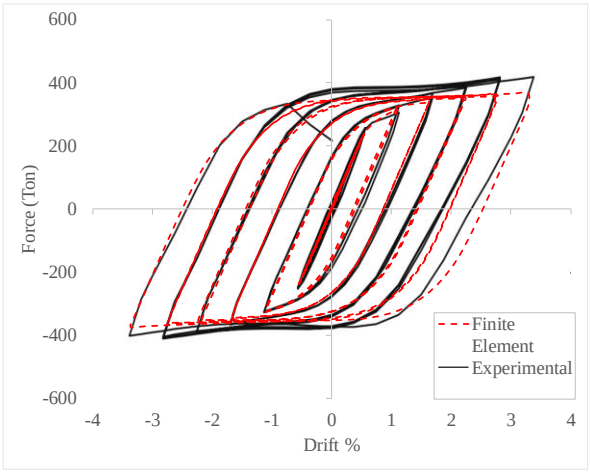

Fig. 7. A comparison between the numerical and experimental models [44,45].

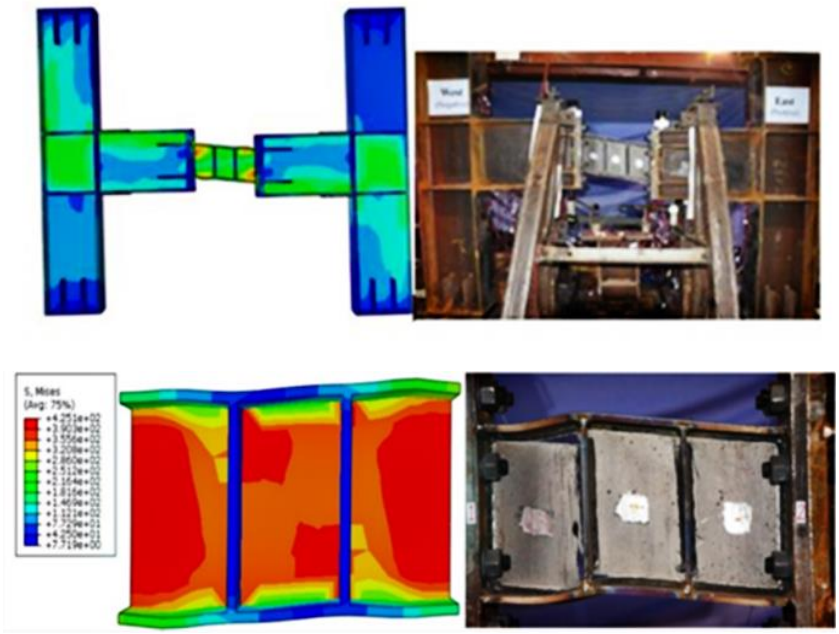

Fig. 8. Comparison between stress distribution in numerical and experimental models [45].

9. Shaped memory alloy materials

This paper studies two models to investigate the effects of SMA in a shear link subjected to the blast load. The control model (i.e., the validated model in the previous section) is used here to compare the results. The shear link model is a model whose shear link is made of the SMA (see Table 3). It should be noted that the properties of the SMA are

selected according to those used in Kamgar *et al.* [53] and introduced as superelastic in the ABAQUS software (see Table 4). Therefore, to investigate the effect of using SMA on the performance of moment frames with replaceable shear links, both models are subjected to an explosion load, and the analysis of the results is presented in the next section. Also, to validate the modeling of SMA in the ABAQUS software, the experimental results on the rebar made of SMA under cyclic loading [54] are compared with the results of numerical modeling in the ABAQUS software. Figure 9 depicts the excellent correlation between experimental and numerical results.

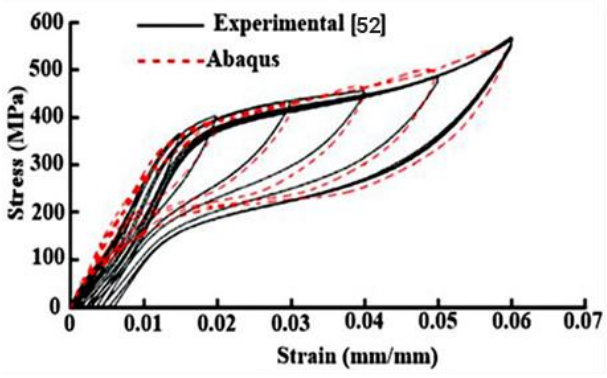

a)

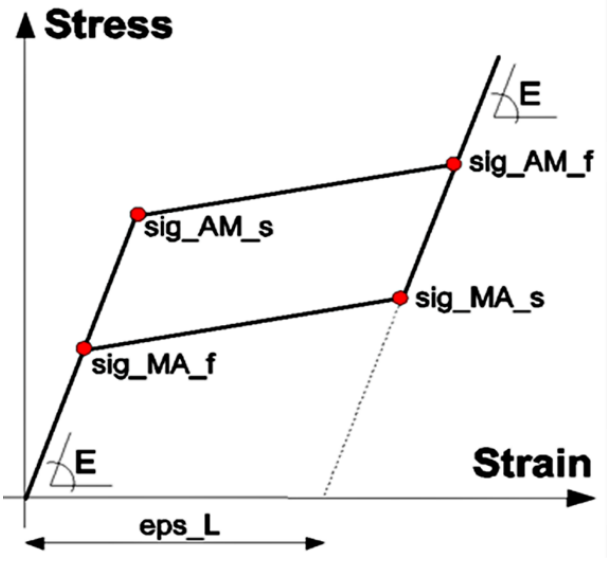

b)

Fig. 9. a) A comparison between the stress-strain curve of the numerical and experimental models b) introduction of different stress and strain points in the stress-strain curve of the SMA.

Table 3. The models under study with their details

Model	Location of SMA material	Details
Control model	-	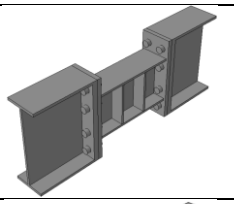
Shear link	Bolts and shear link	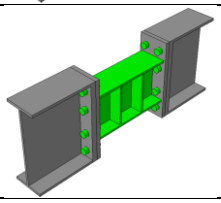

Table 4. The properties of the SMA [52,53].

Material	Parameter	Definition	Value
SMA	E	Elasticity modulus	28 (GPa)
	Y	Poisson ratio	0.3
	sig_AM_s	Austenite to martensite starting stress	330 (MPa)
	sig_AM_f	Austenite to martensite finishing stress	580 (MPa)
	sig_AM_s	Martensite to austenite starting stress	300 (MPa)
	sig_AM_f	Martensite to austenite finishing stress	150 (MPa)

Table (5) shows the first three natural frequencies of the two structures. It can be deduced that SMA has increased the first three natural frequencies of the structure. It should be noted that according to Table (4), the SMA has superelastic and shape memory properties. The SMA is an alloy that can return to its original state after undergoing large deformations. In fact, reversibility can occur by applying heat or removing stress, representing the shape memory and superelastic properties, respectively. Figure (9b) schematically shows the stresses and strains of the SMA presented in Table 4.

Table 5. A comparison between the first three natural frequencies of the studied structures.

Mode	Natural period (sec)	
	SMA	Steel
1	0.0326	0.0321
2	0.0313	0.0311
3	0.0235	0.0185

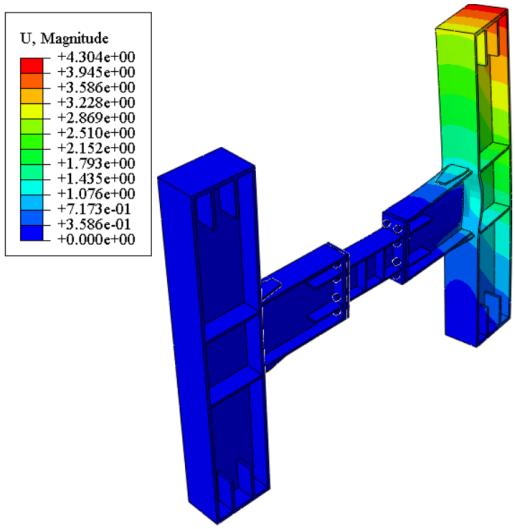

Fig. 10. First mode shape of the frame with SMA shear link.

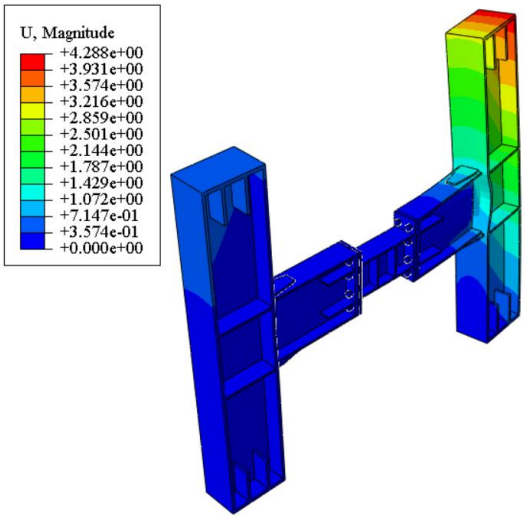

Fig. 11. First mode shape of the frame with steel shear link.

The first mode shapes of the frames with SMA or steel are shown in Figures 10 and 11.

10. Results

After validating the SMA materials and the frame with the shear link under cyclic load, the two models mentioned before (see Table 3) have been utilized here. Therefore, two models are studied and subjected to the three types of blast loads. Finally, the results of Von Mises stress, base shear, and displacement under three blast loads are compared. It should be noted that the total duration of the analysis is 10 μsec, which includes applying the prestressing force of the bolts (one μsec), applying the gravity load (one μsec), and finally, applying the blast load to the structure (eight μsec).

10.1. The results for the blast load type 1

Figures (12-13) show the Von-Mises stresses in the shear link and the frame controlled with the shear link made of ordinary steel and SMA subjected to the blast load type 1.

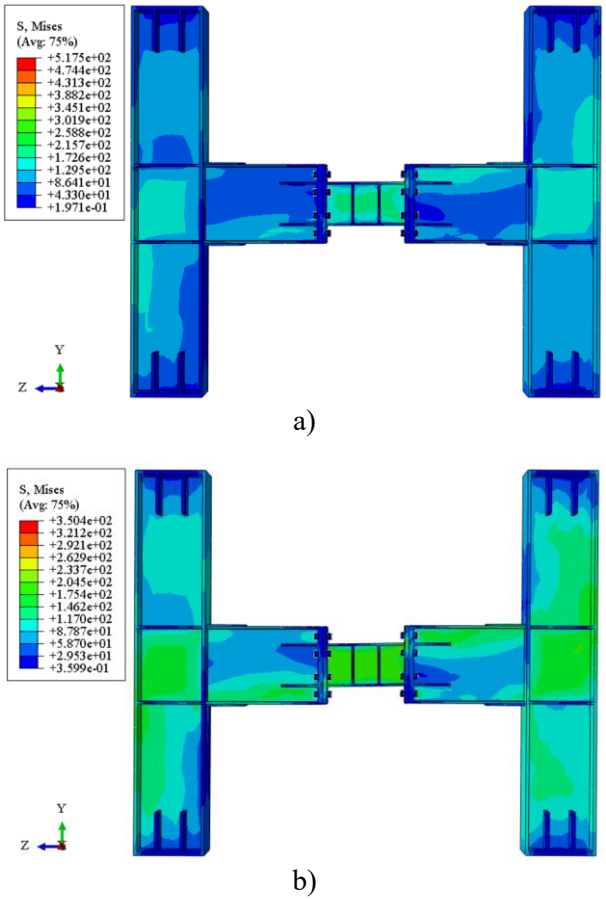

Fig. 12. Von-Mises stresses for a frame with a shear link made of a) ordinary steel and b) SMA under blast load type 1.

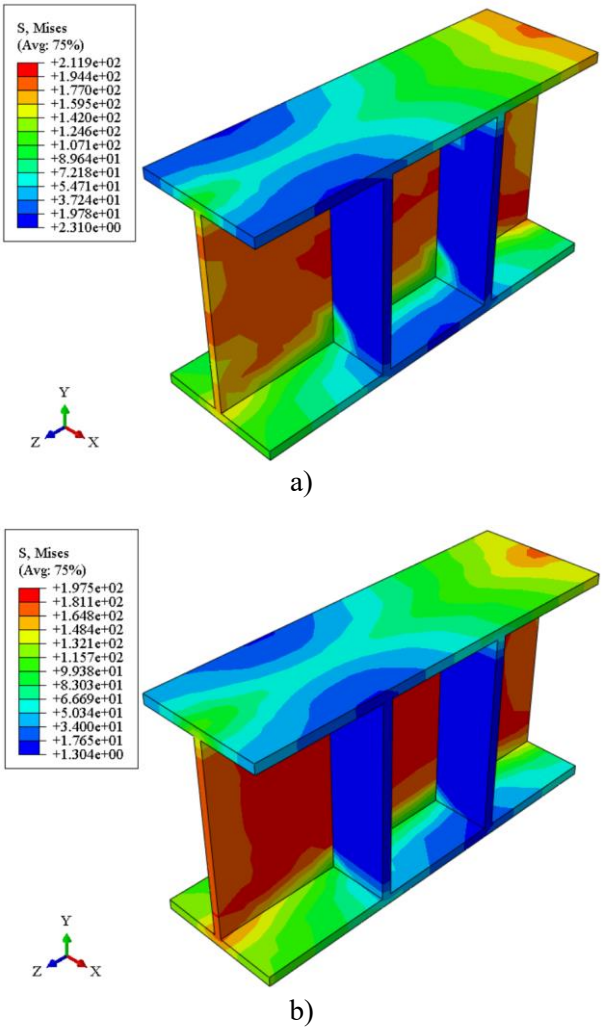

Fig. 13. Von-Mises stresses for the shear link made of a) ordinary steel and b) SMA subjected to the blast load type 1.

From Figures (12-13), it can be concluded that the amount of von Mises stresses in the shear link made of SMA is many times lower than the corresponding values in the shear link made of ordinary steel. Figures (14-15) also show the time history of base shear force and lateral displacement in the frame controlled with the shear link. It is known that the frame equipped with a shear link made of SMA has a lower base shear than the frame controlled by a shear link made of ordinary steel. This leads to a reduction in the cost of the foundation of this frame. Also, the maximum displacement and lateral residual displacement in the frame equipped with a shear link made of ordinary steel are lower than the corresponding values in the frame equipped with a shear link made of SMA.

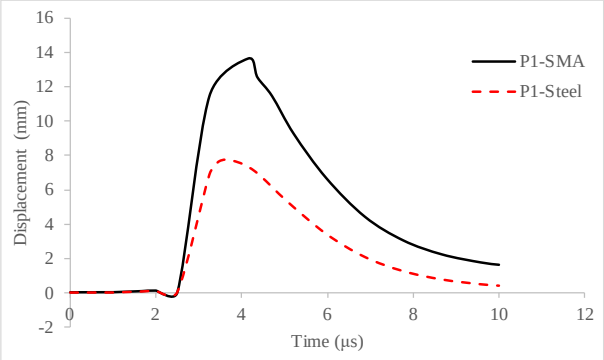

Fig. 14. Comparison of displacement of the frame under blast load (i.e., type 1)

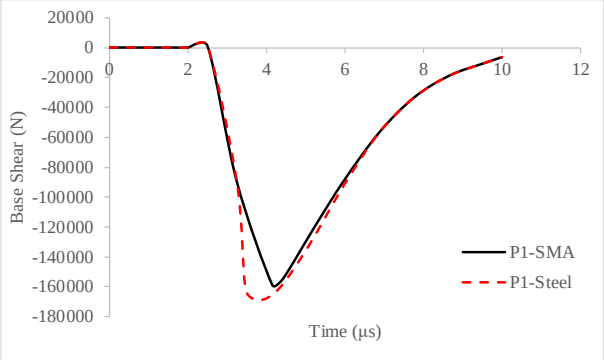

Fig. 15. Comparison of shear force of the frame under blast load (i.e., type 1).

10.2. The results for the blast load type 2

Figures (16-17) show the Von-Mises stresses in the shear link and the frame controlled with the shear link subjected to the blast load type 2.

From Figures (16-17), it can be concluded that the amount of Von-Mises stresses in the shear link in the frame equipped with the shear link made of SMA is still lower than the corresponding values in the shear link made of ordinary steel. Figures (18-19) also show the time history of the base shear and lateral displacement in the frame equipped with the shear link under the blast load type 2.

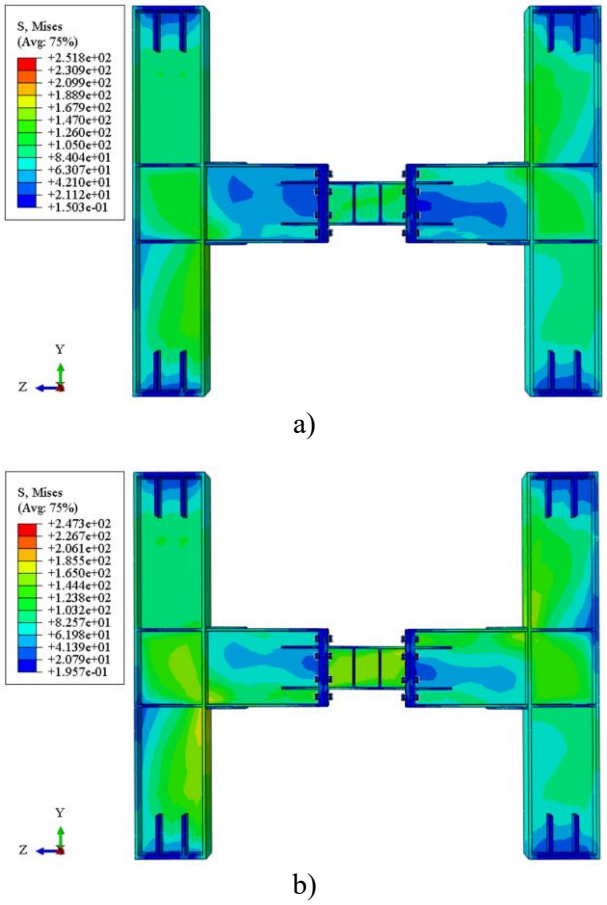

Fig. 16. Von-Mises stresses for a frame with a shear link made of a) ordinary steel and b) SMA subjected to the blast load type 2.

It is clear that in this loading condition, the frame equipped with a shear link made of SMA has a lower base shear than the frame equipped with a shear link made of ordinary steel. Therefore, this leads to a reduction in the cost of the foundation of the building. Also, the maximum displacement in the frame equipped with a shear link made of ordinary steel is less than the corresponding value in the frame equipped with a shear link made of an SMA, while the residual displacement of both frames is the same (both of them are equal to zero).

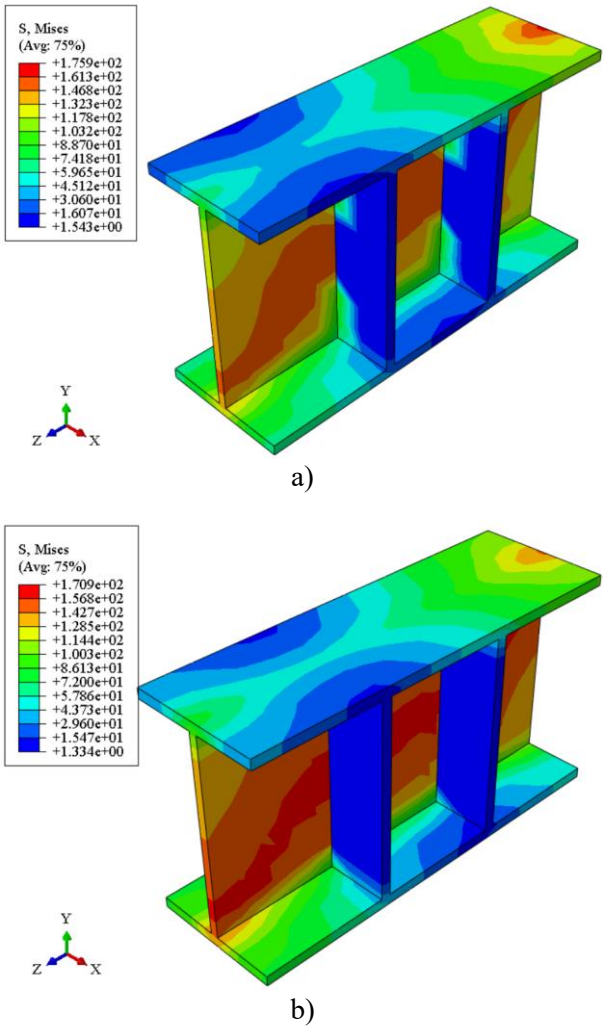

Fig. 17. Von-Mises stresses for a shear link made of a) ordinary steel and b) SMA subjected to the blast load type 2.

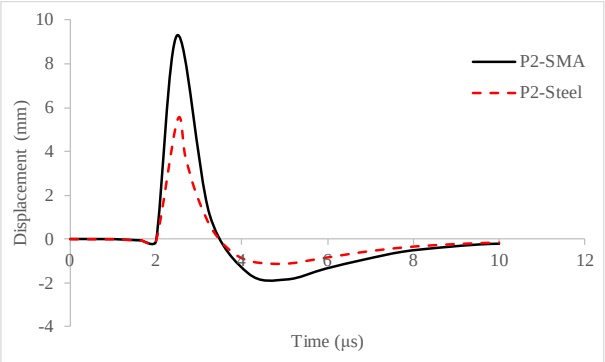

Fig. 18. A comparison between the displacement values of the frame subjected to the blast load type 2.

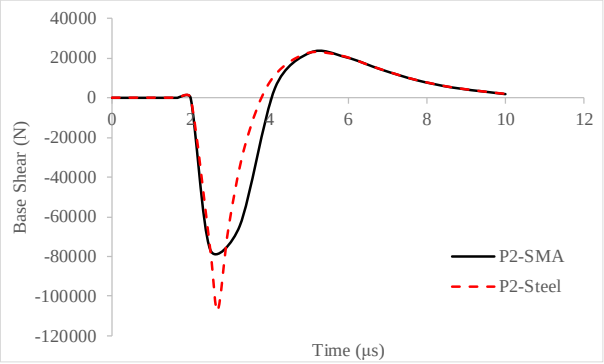

Fig. 19. A comparison between the shear force of the frame subjected to the blast load type 2.

10.3. The results for the blast load type 3

Figures (20-21) show the Von-Mises stresses in the shear link and the frame equipped with the shear link subjected to the blast load type 3.

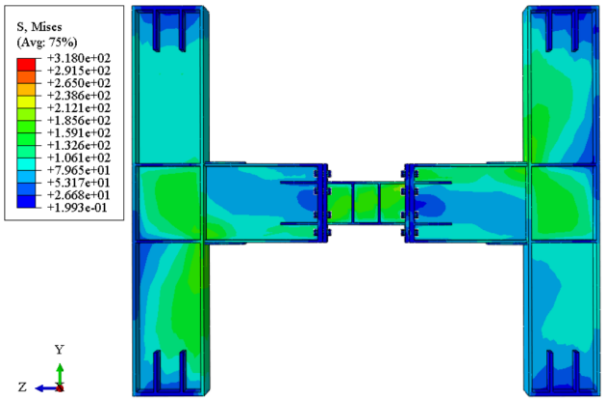

a)

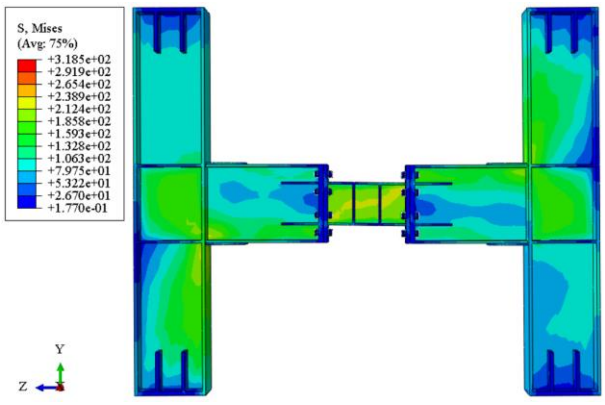

b)

Fig. 20. Von-Mises stresses for a frame with a shear link made of a) ordinary steel and b) SMA subjected to the blast load type 3.

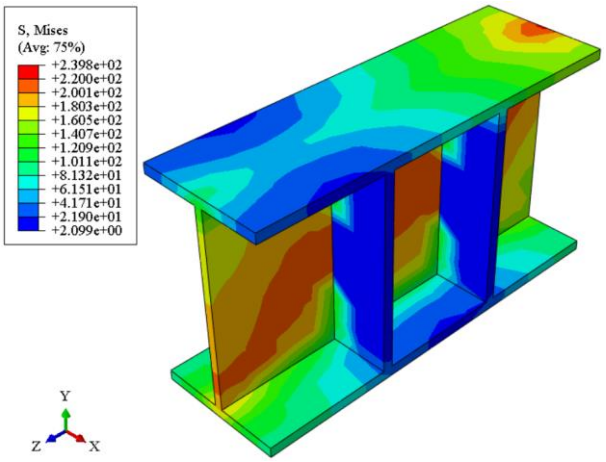

a)

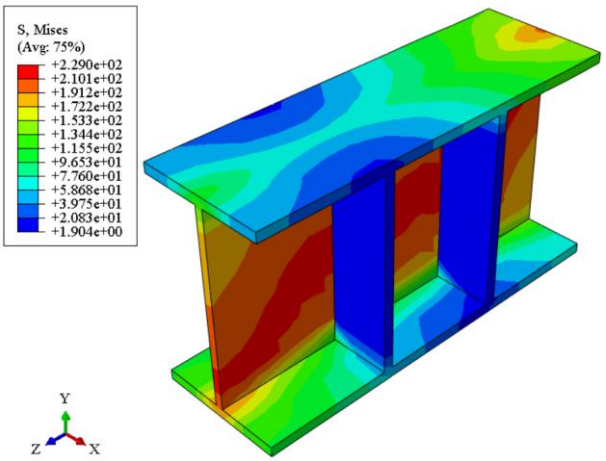

b)

Fig. 21. Von-Mises stresses for a shear link made of a) ordinary steel and b) SMA subjected to the blast load type 3.

From Figures (20-21), it can be concluded that the amount of Von-Mises stresses in the shear link in the frame equipped with the shear link made of SMA is still lower than the corresponding values in the shear link made of ordinary steel. Figures (22-23) also show the time history of base shear and lateral displacement in the frame equipped with the shear link. It is clear that for the mentioned loading type, the frame equipped with a shear link made of SMA has a lower base shear than the frame equipped with a shear link made of ordinary steel, which reduces the foundation's cost. Also, the maximum displacement in the frame equipped with a shear link made of

ordinary steel is less than the corresponding value in the frame equipped with a shear link made of an SMA, while the residual displacement of both frames is the same (both of them are equal to zero).

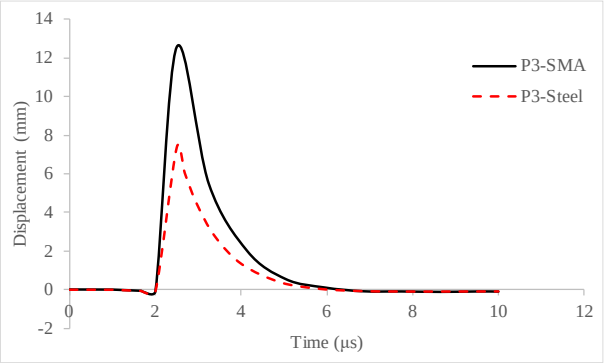

Fig. 22. Comparison of displacement of the frame under blast load type 3.

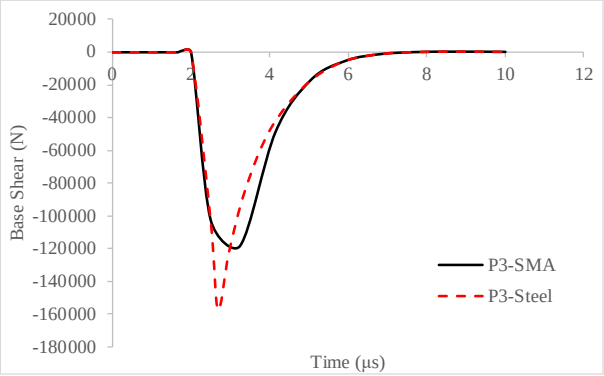

Fig. 23. Comparison of shear force of the frame under blast load type 3.

Also, blast load type 1 has a greater positive and negative force than the other two types, creating a higher base shear than the other two types. Table 6 compares the maximum responses and occurrence times in the studied models under different blast loads. According to Table 6, it is clear that the maximum displacement occurred in the structures equipped with the shear link made of an SMA, while the maximum stress value in these structures is less than the values in the structures equipped with the shear link made of ordinary steel.

Table 6. Comparison of maximum responses and their occurrence time in the studied models.

Blast load	Model	Time (μs)	Disp. (mm)	Time (μs)	Stress (MPa)
Type 1	*SMA*	*4.14*	*13.64*	*4.14*	*197.22*
	OS	*3.47*	*7.63*	*3.47*	*211.91*
Type 2	*SMA*	*2.50*	*9.30*	*2.50*	*170.92*
	OA	*2.50*	*5.45*	*2.50*	*175.87*
Type 3	*SMA*	*2.50*	*12.58*	*2.50*	*229*
	OS	*2.50*	*7.38*	*2.50*	*239.76*

OA refers to ordinary steel.

Figure (24) shows the time history of the maximum stresses in the shear link for the studied models.

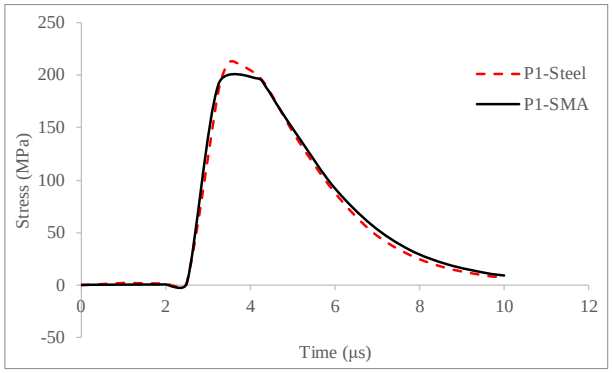

a)

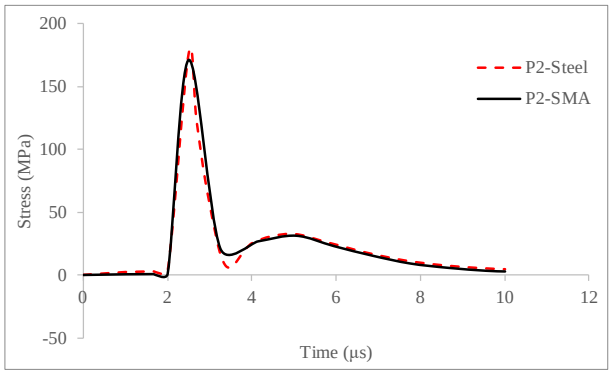

b)

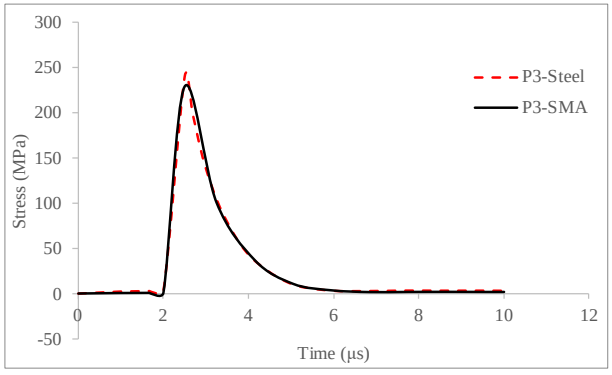

c)

Fig. 24. Comparison of maximum values of stress in the shear link subjected to the blast load for the a) first, b) second, and c) third types.

According to Figure 24, it is clear that with an increase in the positive phase duration of the blast load, initially, the maximum values of the stress have been decreased. Also, these values have been increased again after that.

10.4. A comparison between two frames equipped by shear link made of SMA or ordinary steel under three blast loads

Here, the time history of the displacements and base shear of the structures equipped with shear links made of SMA or ordinary steel under three blast loads is illustrated in Figures 25 and 26.

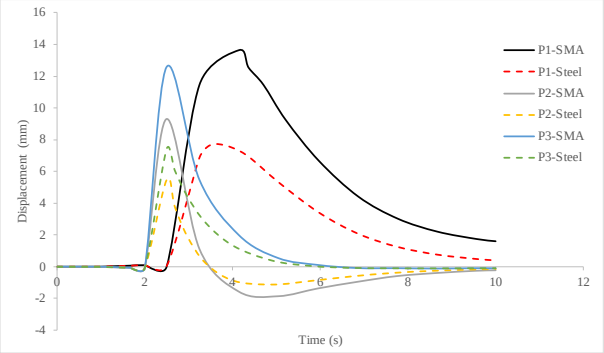

Fig. 25. A comparison between the displacement values.

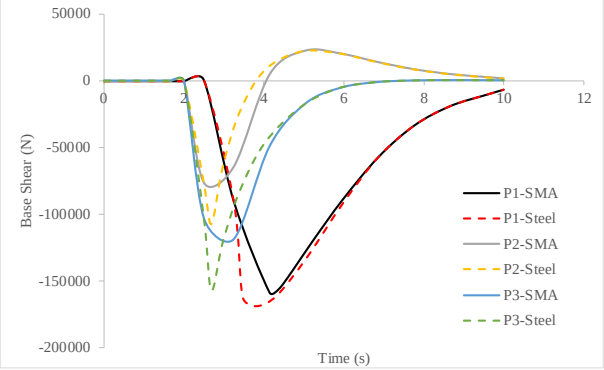

Fig. 26. A comparison between the base shear.

Based on Figures 25 and 26, the maximum displacement and base shear values of different structural systems subjected to different blast loadings have been shown in Figures 27-28.

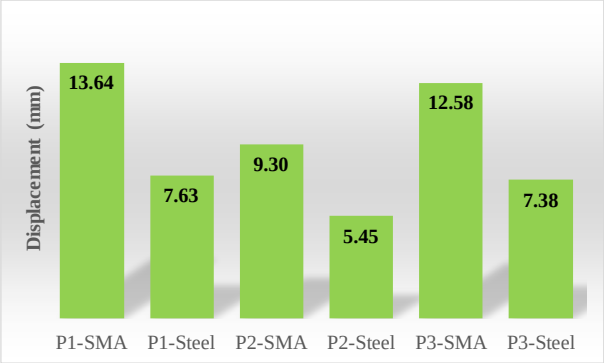

Fig. 27. A comparison between the maximum displacement values for different loading types and structural systems.

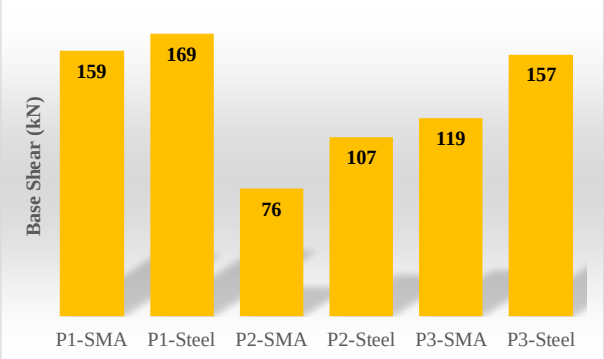

Fig. 28. A comparison between the maximum base shear values for different loading types and structural systems.

Also, Figure 29 compares the maximum stress values of different structural systems subjected to different blast loadings.

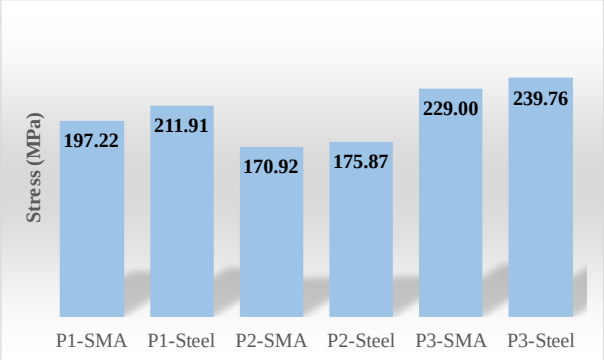

Fig. 29. A comparison between the maximum stress values for different loading types and structural systems.

It can be concluded that for both types of materials (i.e., ordinary steel and SMA), with the increase in the positive phase duration of the blast load, the maximum responses showed a decreasing trend at first. Then an increasing trend can be seen. Also, a comparison between

the SMA and ordinary steel materials shows that the maximum responses of the base shear and Von Mises stress values occur in the frame equipped with the replaceable shear link made of SMA material. The frame controlled by the replaceable shear link made of ordinary steel for maximum displacement responses has fewer values.

10.5. Considering the effect of free vibration after blast loads on the responses of different structures

Here, the effect of free vibration analysis on the maximum responses of the structure has been studied. The time for the free vibration analysis has been considered to be 10 (μsec). Therefore, the total time is 20 (μsec). The damping ratio is considered to be 0.05. As it is clear from Table 7, there is a slight difference between the maximum structure's response considering the free vibration analysis applied after forced vibration and the maximum structure's response without considering the free vibration analysis (see Table 6). Therefore, it can be concluded that the free vibration analysis can be neglected in examining the maximum structure's responses subjected to the blast load.

Table 7. Comparison of maximum responses and their occurrence time in the studied models

Blast load	Model	Time (μs)	Disp. (mm)	Time (μs)	Stress (MPa)
Type 1	*SMA*	*3.50*	*13.72*	*4.00*	*205.17*
	OS	*3.59*	*7.72*	*3.59*	*213.34*
Type 2	*SMA*	*2.50*	*9.30*	*2.50*	*170.91*
	OA	*2.50*	*5.45*	*2.50*	*175.90*
Type 3	*SMA*	*2.50*	*12.58*	*2.50*	*228.81*
	OS	*2.50*	*7.38*	*2.50*	*239.83*

11. Conclusion

Due to the difference in the span length-to-depth ratios of the beams in the framed tube structures, the existing rules proposed by regulations for the moment-resisting frame cannot be utilized directly. This paper proposes a system consisting of a shear link in the middle span of the moment-resisting frame made of SMA. It also examined the behavior of the proposed system under blast load. For this purpose, the effect of three blast loads on the behavior of the framed tube with replaceable shear links made of SMA and conventional steel is investigated. The following results were obtained:

- The frame model with a shear link made of SMA experiences a lower base shear than the frame equipped with a shear link made of ordinary steel. This leads to a decrease in foundation cost for this type of frame (approximately a 25% reduction of the maximum base shear subjected to the blast load type 2 when SMA material was used).
- The maximum displacement values in the frame equipped with a shear link made of ordinary steel are less than those equipped with a shear link made of SMA. There is approximately an increase of 80% of the maximum displacement subjected to the blast load type 2 when SMA material is used. It should be noted that the residual displacement of both frames is the same and equal to zero.
- The maximum stress values in the structure equipped with a shear link made of SMA are less than those in the frame equipped with a shear link made of ordinary steel. There is an approximately 6% decrease in the maximum stress subjected to the blast load type 2 when SMA material is used.
- With an increase in the positive phase duration of the blast load, the maximum response initially decreased and then increased again.
- The cost of the SMA is relatively high. Therefore, using SMA in some parts of the structure that absorb more energy is better and more economical.

- The free vibration has no significant effect on the responses of the mentioned structures under the blast load.

In future research, the response of the complete structure, including the frame with several spans and stories with different arrangements of shear links and connections under various blast loads, can be studied. In addition, the combined effect of fire and explosion on the behavior of this structure can be investigated, too.

Funding

This study has not been funded.

Conflicts of interest

The authors declare that they have no conflict of interest.

Authors contribution statement

Conceptualization, Reza Kamgar, Seyed Ali Mahmoudy and Roham Zakavi; methodology, Reza Kamgar, Seyed Ali Mahmoudy and Roham Zakavi; software, Reza Kamgar and Seyed Ali Mahmoudy; validation, Reza Kamgar and Seyed Ali Mahmoudy; formal analysis, Reza Kamgar and Seyed Ali Mahmoudy; investigation, Reza Kamgar and Seyed Ali Mahmoudy; writing—original draft preparation, Reza Kamgar, Seyed Ali Mahmoudy and Roham Zakavi; writing—review and editing, Reza Kamgar and Seyed Ali Mahmoudy.

References

[1] Reza Kamgar, Noorollah Majidi, Heisam Heidarzadeh. Optimum layout of mega buckling-restrained braces to optimize the behavior of tall buildings subjected to blast load (In Persian). Sci J Adv Def Sci Technol 2020;2:211–30.

[2] Peimani Foroshani S, Hosseini SA. SDOF system solution of the two-way RC slab subjected to blast loading (In Persian). J Adv Def Sci Technol 2021;12:185–96.

[3] Soorani SR, Khosravi F, Sharifi S. Investigation of reinforced soil nail wall behavior against surface blast (In Persian). J Adv Def Sci Technol 2020;10:433–41.

[4] Ngo T, Mendis P, Gupta A, Ramsay J. Blast loading and blast effects on structures - An overview. Electron J Struct Eng 2007;7:76–91. https://doi.org/10.56748/ejse.671.

[5] Magnussa NM, Morrill K. Fast running model for the residual capacity of steel columns damaged by blast & fragment loads. Proc. 79th Shock Vib. Sym., 2008.

[6] Baker JF, Williams EL, Lax D. The Design of Framed Buildings against High-Explosive Bombs. Civ. Eng. War, 1948, p. 3: 80-112. https://doi.org/10.1680/ciwv3.45170.0006.

[7] Luccioni BM, Luege M. Concrete pavement slab under blast loads. Int J Impact Eng 2006;32:1248–66. https://doi.org/10.1016/j.ijimpeng.2004.09.005.

[8] Shi Y, Hao H, Li ZX. Numerical derivation of pressure-impulse diagrams for prediction of RC column damage to blast loads. Int J Impact Eng 2008;35:1213–27. https://doi.org/10.1016/j.ijimpeng.2007.09.001.

[9] Hao H, Wu C, Li Z, Abdullah AK. Numerical analysis of structural progressive collapse to blast loads. Trans. Tianjin Univ., vol. 12, Tianjin, China: Tianjin University; 2006, p. 31–4.

[10] Core RB. Effect of blast load in nonlinear dynamic response of the buckling restrained braces core (In Persian). Sci J Passiv Def Sci Technol 2018;9:107–18.

[11] Tavakoli R, Kamgar R, Rahgozar R. The Best Location of Belt Truss System in Tall Buildings Using Multiple Criteria Subjected to Blast Loading. Civ Eng J 2018;4:1338. https://doi.org/10.28991/cej-0309177.

[12] Mohammad Boheiraee, Mehrnoosh Biglari IA. Numerical assessment of explicit dynamic analysis of structures in severe loading (Case study of three concrete slabs). Bull Earthq Sci Eng 2015;2:13–23.

[13] Amini M, Shojaee S, Rostami S. Inelastic dynamic analysis of structures under blast loads using generalized B-spline method. Asian J Civ Eng 2015;16:183–202.

[14] Khaledy N, Habibi A, Memarzadeh P. A comparison between different techniques for optimum design of steel frames subjected to blast. Lat Am J Solids Struct 2018;15. https://doi.org/10.1590/1679-78254952.

[15] Khaledy N, Habibi AR, Memarzadeh P. Minimum weight and drift design of steel moment frames subjected to blast. Int Joiurnal Optim Civ Eng 2019;9:39–63.

[16] Heydari mal-amiri R, Tavakoli D. Comparison of the behavior of FRP rebar with steel rebar in reinforced concrete columns under impact loading. Civ Infrastruct Res 2021;7:77–91. https://doi.org/10.22091/cer.2021.7062.1260.

[17] Kamgar R, Alipour R, Rostami S. The effect of blast positive impact duration on the maximum responses of a nonlinear dynamic system. Int J Optim Civ Eng 2022;12.

[18] Li M, Zong Z, Hao H, Zhang X, Lin J, Xie G. Experimental and numerical study on the behaviour of CFDST columns subjected to close-in blast loading. Eng Struct 2019;185:203–20. https://doi.org/10.1016/j.engstruct.2019.01.116.

[19] Alavi A, Mele E, Rahgozar R, Noroozinejad Farsangi E, Takewaki I, Málaga-Chuquitaype C. Uniform deformation design of outrigger braced skyscrapers: A simplified method for the preliminary design stage. Structures 2021;31:395–405. https://doi.org/10.1016/j.istruc.2021.01.099.

[20] Amini M, Akbarpour A, Haji Kazemi H, Adibramezani MR. An innovative approach for evaluating mode shapes and natural frequencies of tubular frame and damped outriggers. Innov Infrastruct Solut 2022;7:33. https://doi.org/10.1007/s41062-021-00634-6.

[21] Alavi A, Rahgozar R. A simple mathematical method for optimal preliminary design of tall buildings with peak lateral deflection constraint. Int J Civ Eng 2019;17:999–1006. https://doi.org/10.1007/s40999-018-0349-1.

[22] Davari SM, Malekinejad M, Rahgozar R. Static analysis of tall buildings based on Timoshenko beam theory. Int J Adv Struct Eng 2019;11:455–61. https://doi.org/10.1007/s40091-019-00245-7.

[23] Hasrat HA. Comparative study of various high rise building lateral load resisting systems for seismic load & wind load: A review. Int Res J Eng Technol 2021:291–7.

[24] Sarcheshmehpour M, Estekanchi HE. Life cycle cost optimization of earthquake-resistant steel framed tube tall buildings. Structures 2021;30:585–601. https://doi.org/10.1016/j.istruc.2021.01.038.

[25] Pachideh G, Gholhaki M, Nouri Y. An investigation into the impact of fire on lateral stability and strength of thin steel plate shear walls. Amirkabir J Civ Eng 2020;52:859–72. https://doi.org/10.22060/ceej.2018.15003.5809.

[26] Al-Saadi NTK, Mohammed A, Al-Mahaidi R, Sanjayan J. A state-of-the-art review: Near-surface mounted FRP composites for reinforced concrete structures. Constr Build Mater 2019;209:748–69. https://doi.org/10.1016/j.conbuildmat.2019.03.121.

[27] Sanginabadi K, Yazdani A, Mostofinejad D, Czaderski C. RC members externally strengthened with FRP composites by grooving methods including EBROG and EBRIG: A state-of-the-art review. Constr Build Mater 2022;324:126662. https://doi.org/10.1016/j.conbuildmat.2022.126662.

[28] Wang C, Fan J sheng, Xu L yan, Nie X. Cyclic hardening and softening behavior of the low yield point steel: Implementation and validation. Eng Struct 2020;210:110220. https://doi.org/10.1016/j.engstruct.2020.110220.

[29] Wang M, Fahnestock LA, Qian F, Yang W. Experimental cyclic behavior and constitutive modeling of low yield point steels. Constr Build Mater 2017;131:696–712. https://doi.org/10.1016/j.conbuildmat.2016.11.035.

[30] Wang M, Zhang C, Sun Y, Dong K. Seismic performance of steel frame with replaceable low yield point steel connection components and the effect of structural fuses. J Build Eng 2022;47:103862. https://doi.org/10.1016/j.jobe.2021.103862.

[31] Parvin A, Raad J. Internal and external reinforcement of concrete members by use of shape memory alloy and fiber reinforced polymers under cyclic loading-A review.

Polymers (Basel) 2018;10. https://doi.org/10.3390/polym10040376.

[32] Raza S, Shafei B, Saiid Saiidi M, Motavalli M, Shahverdi M. Shape memory alloy reinforcement for strengthening and self-centering of concrete structures—State of the art. Constr Build Mater 2022;324:126628. https://doi.org/10.1016/j.conbuildmat.2022.126628.

[33] Sultana P, Youssef MA. Seismic performance of modular steel frames equipped with shape memory alloy braces. Bull Earthq Eng 2018;16:5503–27. https://doi.org/10.1007/s10518-018-0394-9.

[34] Askariani SS, Garivani S, Hajirasouliha I, Soleimanian N. Innovative self-centering systems using shape memory alloy bolts and energy dissipating devices. J Constr Steel Res 2022;190:107127. https://doi.org/10.1016/j.jcsr.2021.107127.

[35] Chen ZP, Zhu S, Yu H, Wang B. Development of novel SMA-based D-type self-centering eccentrically braced frames. Eng Struct 2022;260:114228. https://doi.org/10.1016/j.engstruct.2022.114228.

[36] Wang B, Nishiyama M, Zhu S, Tani M, Jiang H. Development of novel self-centering steel coupling beams without beam elongation for earthquake resilience. Eng Struct 2021;232:111827. https://doi.org/10.1016/j.engstruct.2020.111827.

[37] Xu X, Tu J, Cheng G, Zheng J, Luo Y. Experimental study on self-centering link beams using post-tensioned steel-SMA composite tendons. J Constr Steel Res 2019;155:121–8. https://doi.org/10.1016/j.jcsr.2018.12.026.

[38] Liu W, Sun G, Chen L, Kong J. Experimental investigation into NiTi shape memory alloy panels under cyclic shear loading. Eng Struct 2021;245:112958. https://doi.org/10.1016/j.engstruct.2021.112958.

[39] Khosravikhor A, Gholhaki M, Rezaifar O, Pachideh G. Effect of Ni-Ti shape memory alloy on ductility and response modification factor of SPSW systems. Steel Compos Struct 2023;48:353–65. https://doi.org/10.12989/scs.2023.48.3.353.

[40] Weli SS, Gergely VL. Behaviour of smart steel column-beam connection under blast loading. Ce/Papers 2021;4:857–65. https://doi.org/10.1002/cepa.1371.

[41] Weli SS, Vigh LG. Blast performance evaluation of steel moment-resisting frame equipped with smart bolted connection. J Perform Constr Facil 2021;35:4021050. https://doi.org/10.1061/(asce)cf.1943-5509.0001629.

[42] Weli SS, Vigh LG. Blast performance of steel frames equipped with NiTi SMA bolts: design procedure and numerical evaluation. J Struct Eng 2022;148:4022029. https://doi.org/10.1061/(asce)st.1943-541x.0003314.

[43] Weli SS, Vigh LG. Blast reliability assessment and sensitivity analysis of steel MRFs equipped with NiTi SMA bolts. Eng Struct 2023;286:116137. https://doi.org/10.1016/j.engstruct.2023.116137.

[44] ABAQUS. Abaqus 6.11. Dassault Systemes Simulia Corporation, Providence, RI 2011.

[45] Cheng Q, Lian M, Su M, Zhang H. Experimental and finite element study of high-strength steel framed-tube structures with replaceable shear links under cyclic loading. Structures 2021;29:48–64. https://doi.org/10.1016/j.istruc.2020.11.006.

[46] Chaboche JL. Time-independent constitutive theories for cyclic plasticity. Int J Plast 1986;2:149–88. https://doi.org/10.1016/0749-6419(86)90010-0.

[47] Chaboche JL. Constitutive equations for cyclic plasticity and cyclic viscoplasticity. Int J Plast 1989;5:247–302. https://doi.org/10.1016/0749-6419(89)90015-6.

[48] JGJ82-2011. Technical specification for high strength bolt connections of steel structures. Minist Hous Urban-Rural Dev People's Repub China 2011.

[49] Nehdi ML, Ali MAEM. Experimental and numerical study of engineered cementitious composite with strain recovery under impact loading. Appl Sci 2019;9. https://doi.org/10.3390/app9050994.

[50] Gupta S, Stoddart E, Morrison A. Blast resilience enhancement of cable-supported façade utilizing super-elastic shape memory

alloy. J Facade Des Eng 2021;9:1–20. https://doi.org/10.7480/jfde.2021.2.5331.

[51] Sabuwala T, Linzell D, Krauthammer T. Finite element analysis of steel beam to column connections subjected to blast loads. Int J Impact Eng 2005;31:861–76. https://doi.org/10.1016/j.ijimpeng.2004.04.013.

[52] Balden VH, Nurick GN. Numerical simulation of the post-failure motion of steel plates subjected to blast loading. Int J Impact Eng 2005;32:14–34. https://doi.org/10.1016/j.ijimpeng.2005.07.013.

[53] Kamgar R, Heidarzadeh H, Babadaei Samani MR. Evaluation of buckling load and dynamic performance of steel shear wall retrofitted with strips made of shape memory alloy. Sci Iran 2021;28:1096–108. https://doi.org/10.24200/sci.2020.52994.2991.

[54] DesRoches R, McCormick J, Delemont M. Cyclic properties of superelastic shape memory alloy wires and bars. J Struct Eng 2004;130:38–46. https://doi.org/10.1061/(asce)0733-9445(2004)130:1(38).